Air-Hole Properties of Calcite-Filled Polypropylene Copolymer Films

Jagannath Biswas, Hyun Kim, Byung Hyung Lee, Soonja Choe

Department of Chemical Engineering, Inha University, 253 Yonghyundong, Incheon 402-751, South Korea

Received 9 June 2005; accepted 9 March 2006
DOI 10.1002/app.24998
Published online 18 April 2008 in Wiley InterScience (www.interscience.wiley.com).

ABSTRACT: This work was designed to study the effects of inorganic calcite powder on structurally different copolymer [poly(propylene-*co*-ethylene)] and terpolymer [poly (propylene-*co*-ethylene-*co*-1-butene)] matrices and the possibility of making a suitable porous composite film. The yield stress of the composites did not improve, but the modulus increased gradually with the filler loading. The theoretical and experimental modulus and yield stress of the composites provided evidence of filler and polymer adhesion behavior. The impact strength showed little enhancement up to a 20 wt % loading for the poly(propylene-*co*-ethylene-*co*-1-butene) system. The number-average, weight-average, and *z*-average air-hole diameters were compared with respect to the draw ratio as well as the calcite loading. The morphology of a micromechanically deformed composite, studied with an image analyzer, revealed that the aspect ratio and area of the air holes increased linearly as a function of the draw ratio, but the change in the aspect ratio upon filler loading was not remarkable. A suitable loading of a filler up to 30 wt % was good for controlling the porosity in the composite films. © 2008 Wiley Periodicals, Inc. J Appl Polym Sci 109: 1420–1430, 2008

Key words: composites; films; mechanical properties; morphology; phase behavior

INTRODUCTION

Inorganic particulate-filled polymers have been playing a major role in the polymer processing industries. Inert inclusions are added intentionally to the base polymer without sacrificing the processability in an effort to impart various benefits. These materials often replace more than half of the base resin, making the final products cost-effective[1–6] or suitable for special applications.[7–10] Although a recent trend has been focused on inorganic-nanoparticle-filled polymers because they provide better properties with low loadings,[1–14] conventional micrometer-size particulate-filled polymers are still dominant in the market because of their acceptability in many applications. Among the micrometer-size fillers, talc, calcium carbonate, carbon black, and silica have been widely used for a long time in their normal form or surface-modified state.[15–18] Commercially, calcium carbonate is modified by stearic acid ($C_{17}H_{35}$—COOH) and other organic surface modifiers; thus, the hydrophilicity of the surface can be greatly minimized.[19–21] Because polyethylene (PE) and polypropylenes (PPs) are nonpolar and inorganic fillers are generally hydrophilic in nature, the compatibility between them is not favorable. Altering the polarity of the interphase is a unique way of enhancing the properties of particulate-filled composites. Lowering the surface energy is also another way of reducing filler agglomeration in polymer matrices.

In this study, we attempted to make a porous thin film from a polymeric substrate and inorganic calcite. There are several methods available, including the extraction of inorganic fillers from polymers,[22] microphase separation,[23] and mechanical deformation of filled polymers,[24] to make porous structures in polymers. Of the methods mentioned previously, the mechanical deformation method is the cheapest and easiest way. Extraction or solvent mediation for introducing porosity into a film is not environmentally viable at all. Therefore, our focus in this study was the avoidance of any solvent for making composites and the application of micromechanical deformation in the successive stages. These porous films have a wide range of applications in sterile packaging, diaper covers, household wraps, breathable films, and so on. Nago et al.[25] described a calcite-filled porous PP sheet manufacturing process using a simultaneous uniaxial and biaxial stretching technique. A range of calcite particles were selected in their study by the fixing of the stretching ratio and filler content to show the uniformity of the porous structure of the film. A finer pore structure was reported with smaller calcite particles. We elaborated our study in terms of the mechanical properties,

Correspondence to: S. Choe (sjchoe@inha.ac.kr).
Contract grant sponsor: Inha University (2004–2005).

TABLE I
Characteristics of the Resins

Material (grade name)	Code (comment)	Density (g/cm^3)	MI (g/10 min)	HDT (°C)	Supplier
Copolypropylene (R930Y)	CoPP (98 : 2 wt % PP/ethylene)	0.90	4.5	90	SK Corp. (Ulsan, Korea)
Ternary polypropylene (T131N)	TerPP (93 : 2 : 5 wt % PP/ethylene/butylene)	0.90	5.0–5.5	60	SK Corp. (Ulsan, Korea)

HDT, heat distortion temperature; MI, melt index.

morphology of the filler/polymer interface, and quantitative analysis of air holes by varying the calcite content and stretching ratio. Lee et al.[26] developed a nanoporous polymeric film by the mechanical deformation process from PP/PE copolymer blends. On the contrary, our objectives were to use porous films in the field of breathable moisture permeation, and so we directed our study mainly to micrometer-size pores rather than nanosize ones.

This study is the continuation of our series on inorganic calcite and zeolite compounded polyolefins derived by melt processing and subsequent stretching for possible porous film applications.[24] Two copolymers of PP were chosen for their better deformability over PP. Special attention was paid to the morphology of the micromechanically deformed composite films studied with the image analyzer software. The correlation of the theoretical and experimental results was verified by a search for suitable evidence of filler–polymer adhesion. The nature of the air holes in terms of the porous areas, air-hole diameters, and aspect ratios of the composites were also investigated.

EXPERIMENTAL

Materials

The two polymers used in this study were poly(propylene-*co*-ethylene) (CoPP) and poly(propylene-*co*-ethylene-*co*-1-butene) (TerPP), which were supplied by SK Corp. (Ulsan, Korea). The properties of the two selected resins are summarized in Table I, which also includes the physical data of the resins. Inorganic calcite powder was procured from Dowa Chemical Corp. (Tokyo, Japan), and the properties of the calcite are also tabulated in Table II.

Calcite premixing and compounding

The calcite was oven-dried for 2 h at 100°C before mixing, and the resin provided by the supplier was used as received. To obtain a better mix of the calcite and matrices of CoPP or TerPP, the resin/calcite batch was prepared by thorough premixing before it was fed into the hopper of a Brabender laboratory twin-screw extruder (PL 2000, PA) with a length/diameter ratio of 16 as a screw dimension. The mixed compounds, extruded through a round die, were immediately immersed in a cold water bath, and then the solidified, long strands of the composite were pelletized. A temperature gradient, maintained in the twin-screw extruder, was 190°C in the feeding zone, 200°C in the compression zone, 210°C in the metering zone, and 220°C in the die zone for the CoPP system; for the TerPP system, these variables were 180, 190, 200, and 210°C, respectively. The rotation speed of the screw was constantly maintained at 60 rpm for all compositions.

Compression molding

The postcompounded CoPP and TerPP pellets and their composites from the twin-screw extruder were kept in an oven for moisture removal at 105°C for 3 h. All dried pellets were then placed on a Carver laboratory hot press at a pressure of 5×10^4 Pa and a temperature of 200°C for preparing impact bars with dimensions of $3.64 \times 12.7 \times 3.17$ mm^3 according to ASTM D 256. The hot mold was then allowed to cool at room temperature.

Film preparation

The film specimens were prepared by the fixing of a slit die of 100×0.5 mm^2 at the end of the extruder to measure the mechanical and morphological properties. The dimensions of the film were $15 \times 0.4 \times 165$ mm^3 according to ASTM D 882-97 for tensile testing. The extruded film was uniaxially drawn with a take-up device, the film thickness being kept around 0.4 mm.

TABLE II
Properties of the Calcite

Form	Chemical composition	Density (g/cm^3)	Particle size (μm)	Brunauer–Emmett–Teller area (m^2/g)	Modifier	Supplier
Fine, white powder	$CaCO_3$	2.9	1.1	4.8	Stearic acid treated	Dowa Chemical Co. (Japan)

Characterization

The morphology study was done for the purpose of visualizing the wetting status of the matrices by calcite, and image analysis was performed on a drawn film with special software. The dispersion of the calcite in the matrix and the particle agglomeration were visualized from a cryogenically fractured surface, and the morphology of stretched film specimens was analyzed with scanning electron microscopy (SEM; S-4300, Hitachi, Tokyo, Japan). All specimens prepared for the SEM analysis were coated with platinum with a sputter coater before the test.

The tensile properties of the film specimens were measured with an Instron 4465 (MA) at 25°C under 30% humidity. The Young's modulus, yield stress, elongation at break, and maximum stress were enumerated from a stress–strain curve. In particular, the Young's modulus, which is a measure of the stiffness, was compared with the theoretical model. The initial grip distance of the specimens was maintained at 50 mm, and the deformation rate was 50 mm/min. A slow crosshead speed of 5 mm/min on a 2-mm gripped sample was applied to all the composite films for studying the porous morphology.

For mechanical and morphological characterizations, at least 10 specimens were tested, and the most probable results were averaged. The SEM images were used for quantitative analysis of the air-hole diameters, aspect ratio, and area with a special image analyzer and Scion image analyzer software (Scion Corp., Frederick, MD). To avoid complications, the average diameter of the air holes was measured by the conversion of all elliptical air holes to the corresponding spherical diameters. The air-hole diameter was enumerated in terms of the number-average (d_n), weight-average (d_w), and z-average (d_z) diameters according to the following equations (these so-called averages of the air-hole diameter analysis are found elsewhere[27]):

$$d_n = \frac{\sum N_i d_i^1}{\sum N_i} \tag{1a}$$

$$d_w = \frac{\sum N_i d_i^2}{\sum N_i d_i^1} \tag{1b}$$

$$d_z = \frac{\sum N_i d_i^3}{\sum N_i d_i^2} \tag{1c}$$

where N_i is the number of air holes measured arbitrarily from an equal unit of area in the drawn film and d_i is the diameter of the ith particle.

RESULTS AND DISCUSSION

Calcite particles and their dispersions in both matrices

Figure 1(a) presents SEM microphotographs of stearic acid coated calcite particles at 2000× magnification. The size and shape of the calcite particles were irregular in the matrix. The surface of the calcite particle was modified to minimize the agglomeration, but some aggregates were still observed.

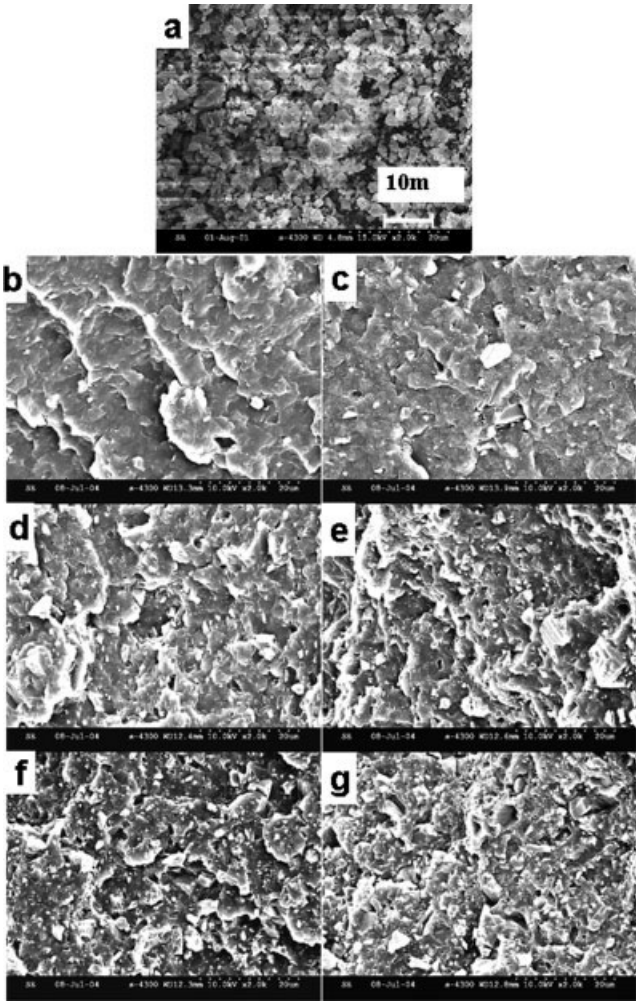

Figure 1 SEM microphotographs (2000×) of (a) stearic acid coated calcite and (b–g) cryofractured surfaces of calcite-filled CoPP composites [(b) 5, (c) 10, (d) 20, (e) 30, (f) 40, and (g) 50 wt %].

To confirm the uniform dispersion and wetting behavior of the calcite particles in all compositions, SEM microphotographs of calcite-incorporated CoPP and TerPP systems were taken with a cryogenically fractured surface. Figures 1(b–g) and 2(a–f) are representations of the cryogenically fractured surfaces of 5, 10, 20, 30, 40, and 50 wt % calcite-filled CoPP and TerPP composites, respectively. Calcite particles were well wetted in the matrices with minimum lumps because a good distributive mixing was achieved during the compounding by means of a twin-screw extruder. With the action of mechanical friction inside the extruder barrel, the initially aggregated particles were reduced to an almost discrete form in CoPP matrices. This was also visible for the

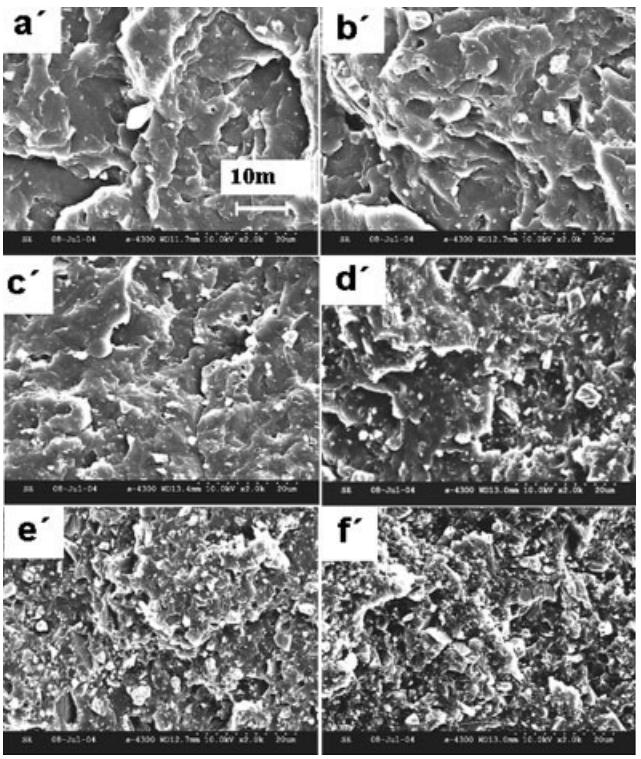

Figure 2 SEM microphotographs (2000×) of cryofractured surfaces of calcite-filled TerPP composites: (a′) 5, (b′) 10, (c′) 20, (d′) 30, (e′) 40, and (f′) 50 wt %.

TerPP matrix and seemed to result in fair adhesion, good wetting being exhibited without remarkable agglomeration.

Mechanical properties

Figure 3 presents the stress–strain curves of pure and calcite-filled CoPP and TerPP film specimens deformed at 50 mm/min [Fig. 3(a,b)]. The yielding behavior was observed for pure and all calcite-filled CoPP and TerPP systems. In general, the yielding phenomenon occurs very close to zero strain for certain polymers, and the initial peak is separately presented in the inset of Figure 3 to avoid confusion. Nonyielding polymers such as elastomers and brittle polymers do not show this type of initial peak. The yield stress was reduced with successive filler loadings for both CoPP and TerPP composites. In addition, 0–20 wt % calcite-filled CoPP and 0–30 wt % calcite-filled TerPP composites showed the elongation at break exceeding 1000% (machine limit; this means that the machine can elongate the sample up to 500 mm) and then declining with further filler loading [Fig. 3(a,b)].

The Young's modulus, which is a characteristic of a material's rigidity, was calculated with the stress–strain curve presented in Figure 4 for CoPP and TerPP, respectively. The experimental moduli of the pure CoPP and TerPP were also plotted with respect to the filler contents, and they were 1084 and 508 MPa, respectively. As the calcite loading increased from 5 to 50 wt % in the CoPP system, the successive increment of the modulus from 1155 to 2018 MPa was observed. On the other hand, the Young's modulus of the TerPP system increased from 571 to 1150 MPa for identical calcite incorporation. It is well known that the inclusion of a rigid particulate filler induces an increase in the stiffness and Young's modulus of composites.[2,6]

Several theories have been presented for evaluating composite properties that depend on the modulus of the filler and filler volume fraction. One of the physical properties, such as the modulus, of the filled materials could be derived from a simple rule of mixtures, which is given here for a binary mixture:[28]

$$E_c = E_p\phi_p + E_f\phi_f \quad (2)$$

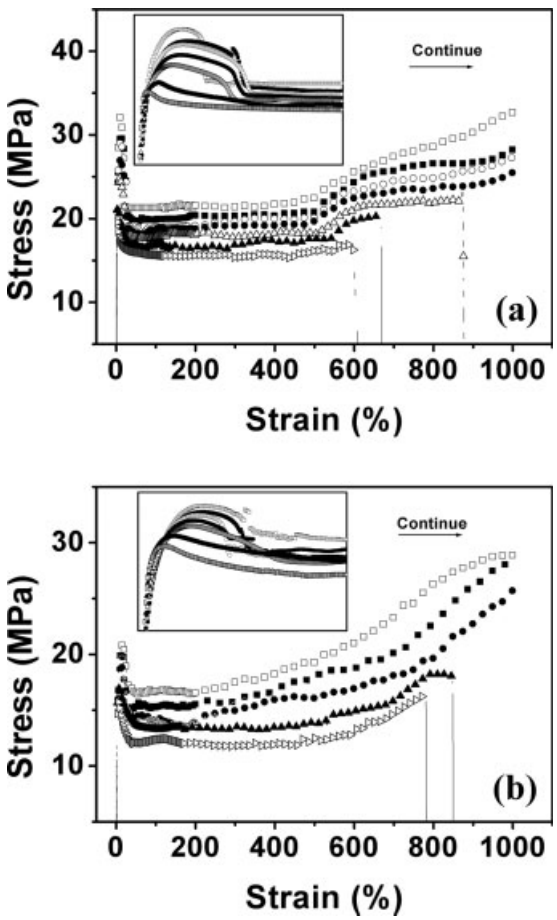

Figure 3 Stress–strain curves of film specimens for pure and calcite-filled (a) CoPP and (b) TerPP composites at crosshead speeds of 50 mm/min: (–□–) pure, (–■–) 5% calcite, (–○–) 10% calcite, (–●–) 20% calcite, (–△–) 30% calcite, (–▲–) 40% calcite, and (–□–) 50% calcite.

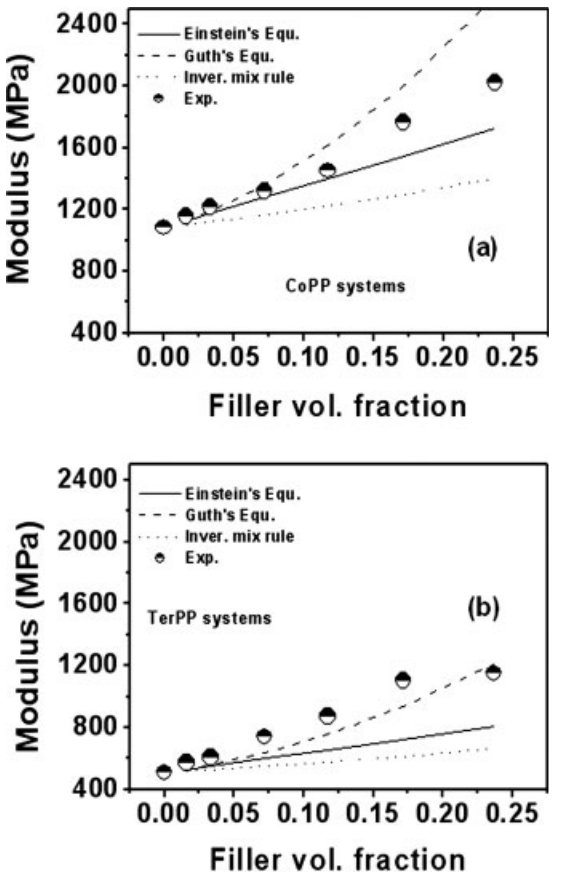

Figure 4 Verification of the experimental and theoretical moduli of pure and calcite-filled systems: (a) CoPP and (b) TerPP (Einstein's equation, Guth's equation, inverse mixing rule, and experimental data).

where E_c is the modulus of the composites; E_p and E_f are the moduli of the polymer matrix and filler, respectively; and ϕ_p and ϕ_f are the volume fractions of the polymer and filler, respectively. Also, the inverse rule of mixtures,[28] another way of expressing moduli found in the literature, has the following form:

$$E_c = \frac{E_p E_f}{E_p \phi_f + E_f \phi_p} \tag{3}$$

Equation (2) is appropriate when strong adhesion exists between the filler and polymer and the filler has a higher aspect ratio, whereas eq. (3) is applicable to rigid spherical particles.

Two more models deriving the modulus of particulate-filled composites were also applied here for experimental data comparison. The simplest one, introduced by Einstein, has the following form:[9]

$$M_c = M_p(1 + 2.5\phi) \tag{4}$$

where M_c, M_p, and ϕ are the moduli of the elasticity of the composite and unfilled polymer and the volume fraction of the filler, respectively. This equation is valid for low filler loadings, assuming perfect adhesion between the filler and polymer matrix. Einstein's equation implies that the stiffening action of the filler is independent of the particle size of the filler. It follows only the volume occupied by the filler and neglects the filler weight. On the other hand, moduli of composites described by eqs. (2) and (3) depend on individual moduli of the filler and pure matrices and the volume fractions of both components (the modulus of calcite particles was taken to be 50 GPa).

An extension of Einstein's theory for enumerating the composite modulus was derived by Guth and Smallwood:[11]

$$M_c = M_p(1 + 2.5\phi + 14.1\phi^2) \tag{5}$$

where all notations are the same as those in the previous equation.

The calculation of the filler volume and resin concentration is based on the solid densities of the constituents. The relationship between the volume fraction (ϕ) and weight fraction (f) of the filler in the composite is represented by

$$\phi = \frac{\varphi}{\varphi + (1 - \varphi)\frac{\eta_f}{\eta_p}} \tag{6}$$

where η_f and η_p are the densities of the filler and pure polymer, respectively.

We calculated the moduli, using eqs. (2)–(4), and plotted them in Figure 4. Figure 4(a) presents the CoPP/calcite system; the experimental data are found in the middle between the theoretical values of the Einstein[9] and Guth[11] equations, but they are higher than the values calculated by the inverse rule of mixtures. Because the surface of the calcite particles was coated with stearic acid, the wetting between the calcite and CoPP matrix seemed better than what we found in our previous study on zeolite-filled CoPP.[29] On the contrary, for the TerPP/calcite system [Fig. 4(b)], the experimental data deviated more positively from all three theoretical equations. This positive deviation may have been the result of stronger adhesion with calcite than with CoPP/calcite systems. The higher experimental modulus of the TerPP/calcite systems is obviously due to the presence of a butylene comonomer as well as the low surface energy of the treated filler. It is not easy to directly measure the adhesion parameter between the calcite and polymer under this experimental condition. Many other factors may have an indirect influence on it. Some other researchers also found an anomalous result when they verified the modulus of filled systems by a theoretical model.[30]

Figure 5(a) shows the yield stress of pure CoPP and TerPP and their composites as a function of the

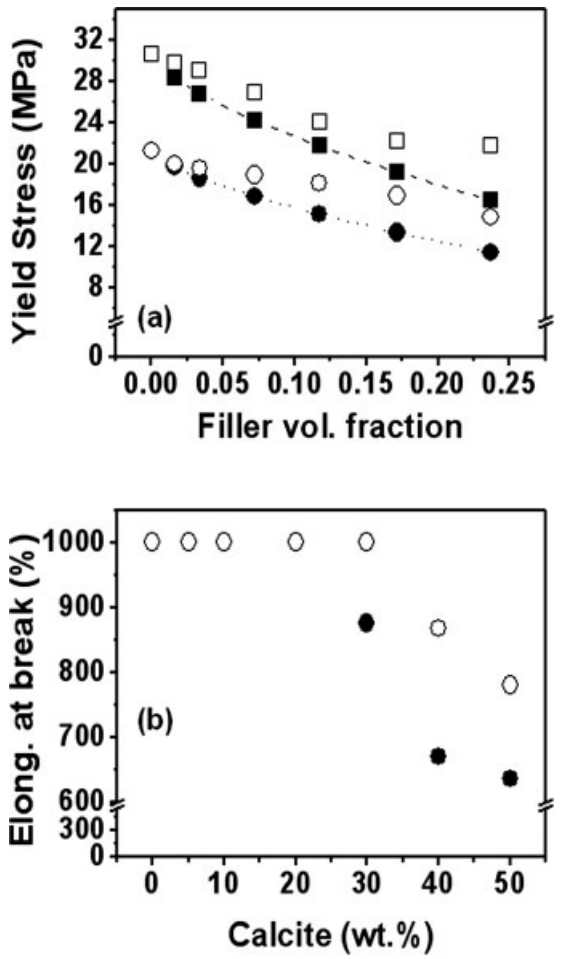

Figure 5 (a) Yield stress comparison according to the Nicolais–Narkis model for pure and calcite-filled (■,□) CoPP and (●,○) TerPP systems (solid symbols represent theoretical values; open symbols represent experimental values) and (b) elongation at break for pure and calcite-filled (●) CoPP and (○).

filler content. The initial yield stresses of the neat samples were 31 and 21.5 MPa, which decreased to 22 and 15 MPa by the successive loading of calcite in CoPP and TerPP, respectively. The yielding phenomena of filled polymers have been reported by several authors with the same view.[30–32] Between the two systems, the yield stress of the TerPP/calcite system was lower than that of the CoPP system. This behavior may have arisen from the 1-butene in the TerPP system, which lowered the stress upon the incorporation of the rubber-type component. Thus, the difference in the yield stress between the two systems clearly resulted from the structural dissimilarity of the matrices upon the addition of a comonomer.

Also in Figure 5(a), the experimental yield stresses of both systems are compared with theoretical values and plotted against the volume fraction of the filler. One of the yield stress models of the composite, which was proposed by Nicolais and Narkis,[34] is represented as follows:

$$\sigma_{yf} = \sigma_{yp}(1 - b\phi^{2/3}) \quad (7)$$

where σ_{yf} and σ_{yp} are the yield stresses of the composite and unfilled polymer, respectively, with the volume fraction of filler (ϕ) being the same as in the previous equations. The factor b accounts for the adhesion quality between the matrices and the inclusions. We calculated the yield stress of each composite at $b = 1.21$, which is the extreme case of poor adhesion for spherical inclusions. In general, the lower the value of b was below 1.21, the stronger the adhesion was.[25] The theoretical values were lower than our experimental values for both the CoPP and TerPP composites. The higher experimental yield stress indicated better adhesion than we predicted, and the tendency was similar for both the CoPP and TerPP systems. Lyu et al.[30] reported on the yielding behavior of composites in terms of their experimental slope. The lower the slope, the better the adhesion will be. The observed slope in our experimental curve is lower than the theoretical one. In addition, TerPP composites yielded a slightly lower slope than the CoPP system, and this presumably indicates better adhesion of calcite with TerPP than with CoPP.

The elongation at break, drawn in Figure 5(b), was more than 1000% for up to a 20% calcite loading and 875, 670, and 635% for 30, 40, and 50 wt % calcite-filled CoPP systems, respectively. In addition, it was more than 1000% for up to 30 wt % calcite and 867 and 780% for 40 and 50 wt % calcite-filled TerPP systems, respectively. The elongation values were similar up to a 20 wt % loading, and beyond this, the TerPP system showed slightly higher elongation. The structural variation of the terpolymer, which had an additional rubbery microstructure of 1-butene, played a vital role in the ultimate elongation of the film. The discontinuity and stress concentrations, due to the rigid inclusions in the matrices, were generally responsible for the reduced elongation at higher filler loadings.

Impact properties

Figure 6 presents a graphical representation of the impact strength of both CoPP and TerPP systems, with experimental deviations shown by an error bar. The impact strength of the CoPP composites did not improve with the addition of calcite, but the TerPP systems showed a higher impact strength than the corresponding unfilled system with up to a 20 wt % calcite loading. In addition, the impact strength of the TerPP system was higher than that of the CoPP system, and this implied that the incorporation of 1-butene was responsible for this behavior, which was

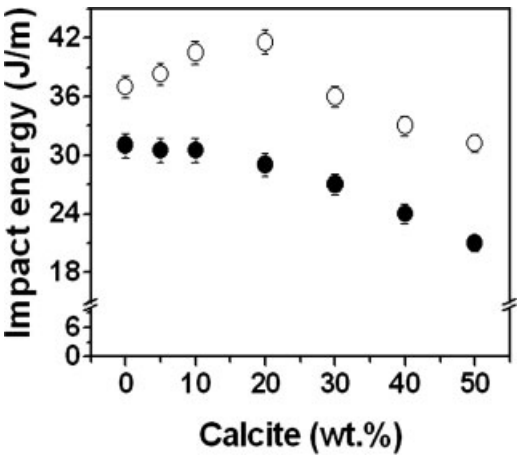

Figure 6 Impact properties of pure and calcite-filled systems at room temperature: (●) CoPP and (○) TerPP.

consistent with the mechanical properties. In general, the impact property has no positive effect when part of the rubbery phase is substituted from matrices with a rigid inert filler or inclusions. The impact strength of the TerPP/calcite composite was different from that of the TerPP/zeolite composite, but reduced impact strength for calcite- or zeolite-filled CoPP composites was observed.[29]

Quantitative analysis of air holes by image analysis

The comparative drawn morphology of 30 wt % calcite-filled CoPP with draw ratios of 0.5, 2.0, 3.0, and 4.0 is shown in Figure 7(a–d), respectively, and Figure 7(a′–d′) presents the TerPP system with the same draw ratio. At the lowest draw ratio of 0.5, the dewetting was just initiated between the calcite particles and the matrices [Fig. 7(a,a′)]. However, as the applied draw ratio increased, the size of the previously formed air holes continued to grow in the machine direction, regardless of the systems. In addition, the initially formed air holes were continuously enlarged along the machine direction upon uniaxial stretching.

In an article published by Nago et al.[25] on stretched PP/$CaCO_3$ composite sheets made with a biaxial stretching technique, they investigated the microstructure in relation to the $CaCO_3$ particle size in the range of 0.08–3.0 μm. It was emphasized that the effective porosity increased and the tortuosity factor and equivalent size of the pore became smaller with the decreasing mean particle size of the filler. In another investigation, Mizutani et al.[33] also reported that the pore size and porosity were controllable by the adjustment of the filler content, particle size of the filler, and degree of stretching. Some of their results can be presented as follows: with decreasing particle size, fine particles are apt to aggregate much more and result in a wider particle size distribution and broader pore size distribution of the microporous PP sheet. Evidently, the use of a filler with a smaller particle size makes it possible to prepare a microporous sheet with a finer pore structure. Our results with respect to air holes in composite films were also thoroughly analyzed and are presented in the next section.

The image analyzer software was used for quantitative measurements of SEM images. The average aspect ratio of air holes, total area of the air holes, and diameter of the air holes upon stretching were calculated with a 30 wt % content loading and various draw ratios. To analyze the morphological properties of the CoPP and TerPP composites, the comparative

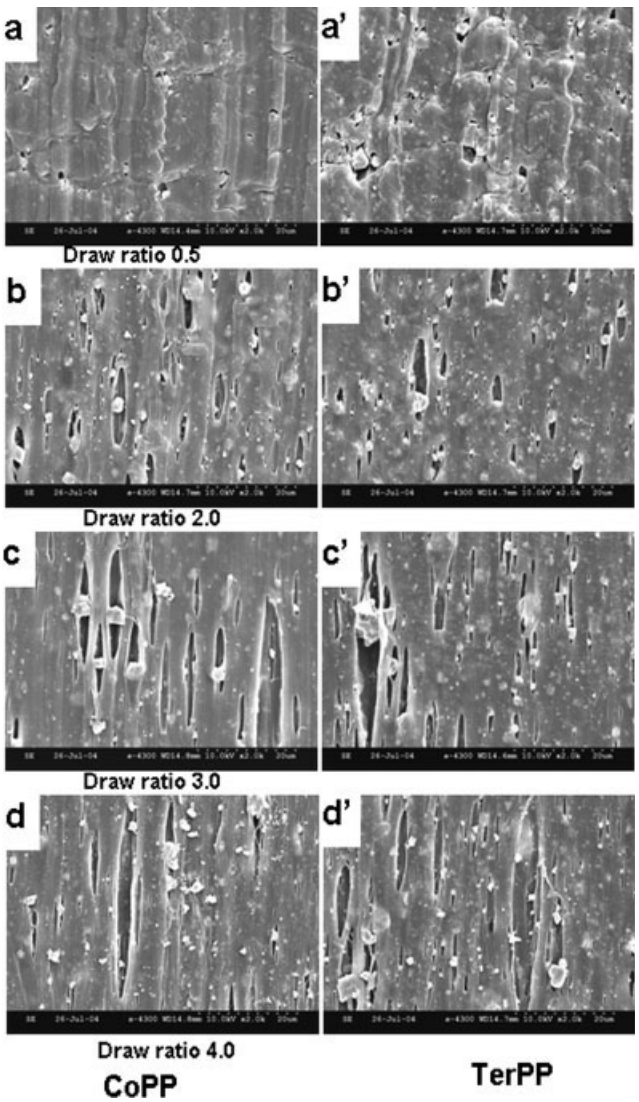

Figure 7 SEM photographs of 30 wt % calcite-filled (a–d) CoPP and (a′–d′) TerPP composite films stretched at different draw ratios (0.5, 2, 3, and 4).

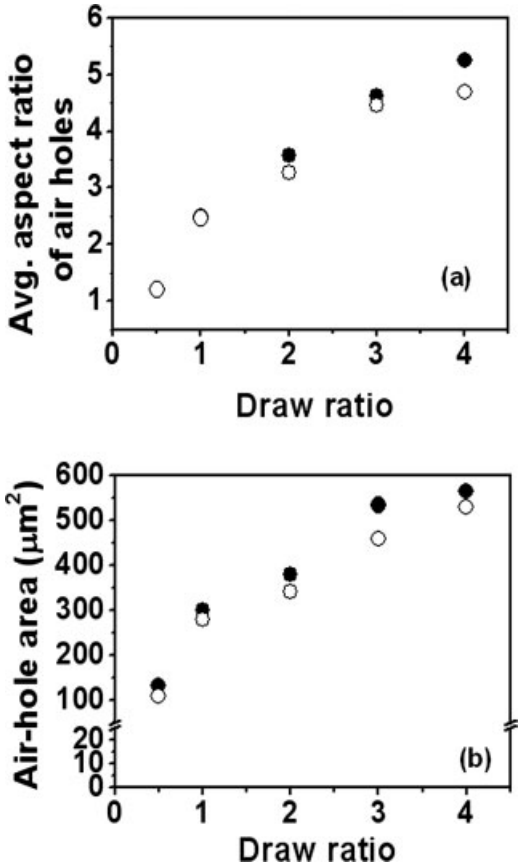

Figure 8 (a) Aspect ratio and (b) total area of the air holes of 30 wt % calcite-filled (●) CoPP and (○) TerPP composite films as a function of the draw ratio.

values of the aspect ratio and total area of the air holes are plotted in Figure 8(a,b), respectively, for 30 wt % calcite-filled systems with various draw ratios. In Figure 8(a), the values of the air-hole aspect ratio (the ratio of the major axis to the minor axis of the air hole) linearly increase with the draw ratio. The observed average aspect ratio increases from 1.22 to 5.25 for the CoPP system and from 1.2 to 4.7 for the TerPP system. The result is analogous to that of our previous report on zeolite-filled CoPP and TerPP systems.[29] The lower aspect ratio of the TerPP system versus that of the CoPP system can be explained by its microstructural differences. The rubbery and glassy behavior of the polymer matrix may be influencing the aspect ratio of the air holes. At equal drawings, the stiff matrix yielded a higher aspect ratio than the soft matrix.

In Figure 8(b), the total area of the air holes in both the CoPP and TerPP systems according to the draw ratio shows successive increments up to the maximum draw ratio of 4. The air-hole area of the CoPP system was slightly larger than that of the TerPP system. The total area of the air holes was calculated to be 2700 μm^2, as analyzed from the image area for every composition.

The image-analyzed number-average, weight-average, and *z*-average air-hole diameters were measured quantitatively according to eq. (1) and are plotted in Figure 9. The number-average air-hole diameter, as shown in Figure 9(a), increased from 1.07 to 2.5 μm and from 0.98 to 2.16 μm for the calcite-filled CoPP and TerPP, respectively, within the draw ratio range of 0.5–4.0. Our previous report showed a similar outcome.[9] In Figure 9(b,c), similar trends for the weight-average and *z*-average diameters of the air holes for both systems can be observed. The weight-average air-hole diameter increased from 1.2 to 4.41 for the CoPP system and from 1.15 to 4.18 μm for the TerPP system between the draw ratios of 0.5–4.0. On the other hand, the *z*-average air-hole diameter increased from 1.65 to 8.01 μm and from 1.53 to

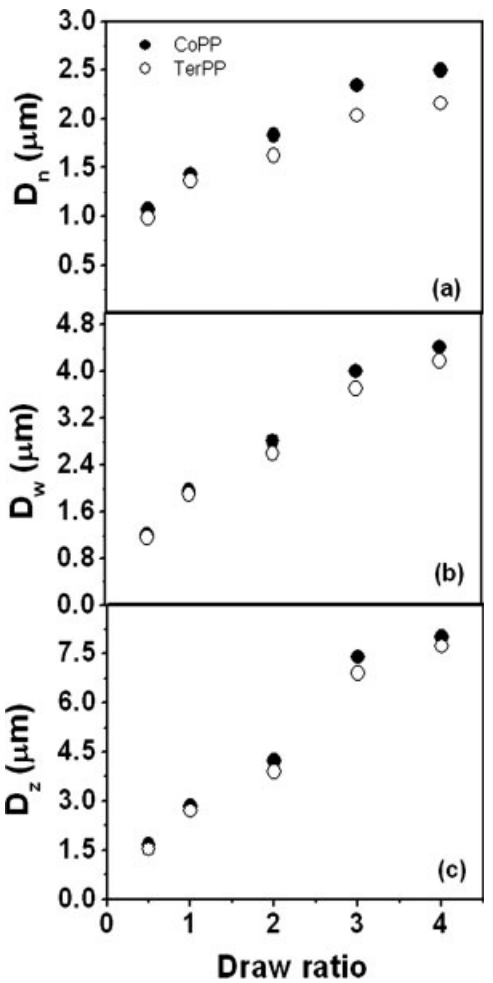

Figure 9 (a) Number-average (D_n), (b) weight-average (D_w), and (c) *z*-average (D_z) diameters of air holes of 30 wt % calcite-filled (●) CoPP and (○) TerPP porous films versus the draw ratio.

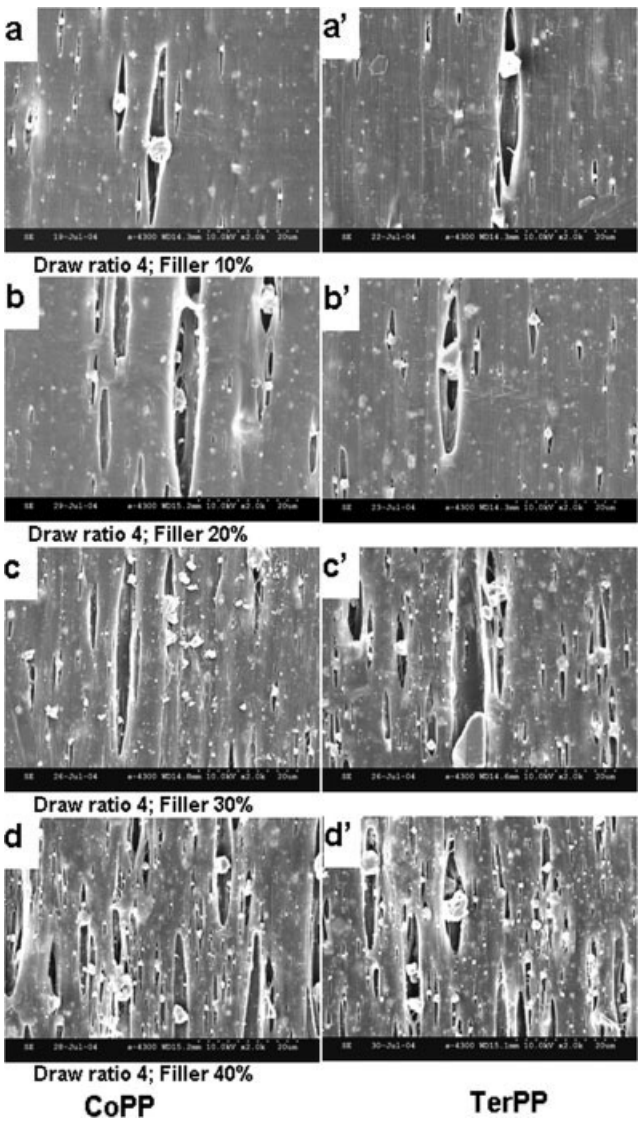

Figure 10 SEM morphology of 10, 20, 30, and 40 wt % filled films stretched at a fixed draw ratio of 4.0: (a–d) CoPP and (a′–d′) TerPP.

7.73 μm for the CoPP and the TerPP systems, respectively, within the same drawing limit.

Figure 10 presents the comparative drawn morphology of the CoPP and TerPP systems with various calcite contents at a constant draw ratio of 4.0. The SEM photographs in Figure 10(a–d,a′–d′) represent a few compositions of the drawn films of CoPP and TerPP containing 10, 20, 30, or 40 wt % calcite, respectively.

The aspect ratio and total area of the air holes are also plotted in Figure 11(a,b), respectively, as a function of the calcite content at a fixed draw ratio of 4.0. The average air-hole aspect ratio lay between 4.58 and 5.65 for all compositions, and this indicated that the filler content did not remarkably influence the aspect ratio. In Figure 11(b), the total area of the air holes in both the CoPP and TerPP systems is plotted as a function of the calcite content at a fixed draw ratio of 4.0. The total area of the air holes in both systems gradually increased with the calcite loading and was maximized at a 50 wt % loading.

The number-average, weight-average, and *z*-average air-hole diameters are also presented in Figure 12 with respect to the calcite content at a fixed draw ratio of 4.0. The number-average air-hole diameter, as shown in Figure 12(a), lay between 2.37 and 3.3 μm and 2.16 and 3.1 μm for calcite-filled CoPP and TerPP, respectively. As shown in Figure 12(b), the weight-average air-hole diameter fluctuated between 4.17 and 5.4 μm and 4.01 and 4.75 μm for the CoPP and TerPP systems, respectively. Finally, the *z*-average air-hole diameter [Fig. 12(c)] varied from 7.52 to 8.78 μm and from 7.42 to 8.22 μm for the CoPP and TerPP systems, respectively.

Overall, the image-analyzed results show that 40 and 50 wt % filled films produced higher air-hole areas, but the elongation was more influenced by these concentrations. Moreover, the changes in the average air-hole diameters and aspect ratios were almost invariable with the filler content. Therefore, a

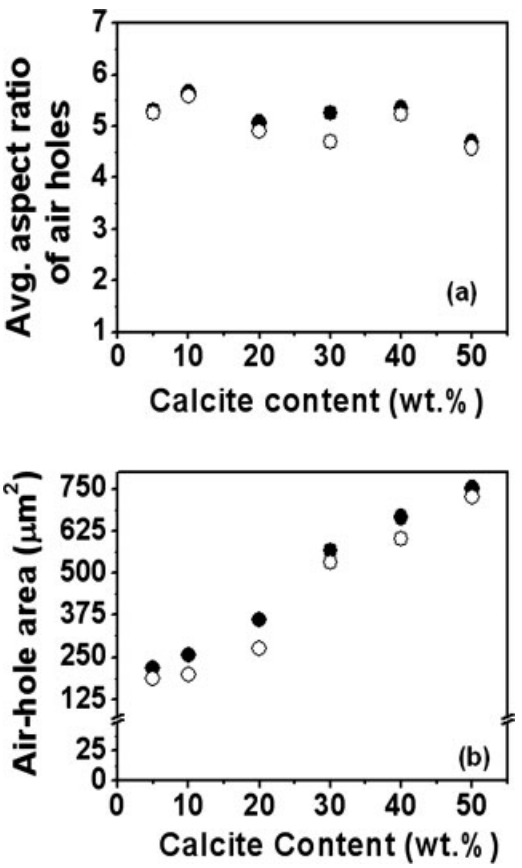

Figure 11 (a) Aspect ratio and (b) total area of the air holes of (●) CoPP and (○) TerPP composite films as a function of the filler content at a fixed draw ratio of 4.0.

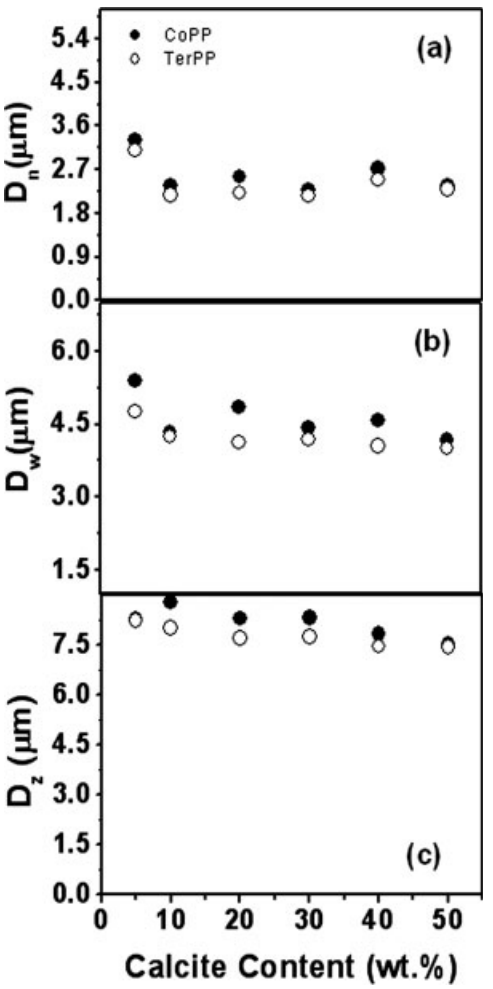

Figure 12 (a) Number-average (D_n), (b) weight-average (D_w), and (c) *z*-average (D_z) diameters of air holes as a function of the filler loading at a constant draw ratio of 4.0: (●) CoPP and (○) TerPP.

loading up to 30 wt % would be suitable for controlling the porosity in the composite films.

CONCLUSIONS

Inorganic-calcite-filled CoPP and TerPP composites were prepared by melt extrusion, by which their films were micromechanically deformed, and this resulted in the microporosity of the films. As this method avoids all sorts of solvents, it will be cost-effective, nontoxic, and environmentally sustainable for manufacturing porous films for sterile packaging, diaper covers, household wraps, breathable films, and so forth. An improved Young's modulus was observed with successive increments of the filler in both systems. The yield stress of the CoPP and TerPP films gradually decreased with successive calcite loadings, but it showed little positive deviation in comparison with the theoretical model. Better adhesion with the polymer and filler were reported from the yield stress and study of the experimental and theoretical moduli. The elongation at break was almost constant up to a certain loading but was reduced at higher filler concentrations in both systems. The impact strength of the composites did not show any improvement over that of the pure components, although it increased for TerPP composites up to a 20 wt % filling. The aspect ratio and the area of the air holes increased almost linearly with the draw ratio. Number-average, weight-average, and *z*-average quantitative air-hole diameters linearly increased with the draw ratio but were almost invariable as a function of the loading. The changes in the average air-hole diameters and aspect ratios were almost invariable with the filler content, and so a loading up to 30 wt % would be suitable for controlling the porosity in the composite films. Our experimental results, based on the use of calcite, a widely used and low-cost filler, will be good guidelines for manufacturing breathable, microporous films and selecting appropriate matrices.

This work is financially supported by Inha University.

References

1. Hale, W. R.; Dohrer, K. K.; Tant, M. R.; Sand, I. D. Colloid Surf A 2001, 483, 187.
2. Nielsen, L. E.; Landel, R. F. Mechanical Properties of Polymers and Composites; Marcel Dekker: New York, 1994.
3. Verbeek, C. J. R. Mater Lett 2002, 52, 453.
4. Bai, S. L.; Chen, J. K.; Huang, Z. P.; Liu, Z. D. Polym Int 2001, 50, 222.
5. Wang, G.; Jiang, P.; Zhu, Z.; Yin, J. J Appl Polym Sci 2002, 85, 2485.
6. Kocsis-Karger, J. Polypropylene Structure, Blends and Composites; Chapman & Hall: London, 1995.
7. Mihai, R.; Nicoleta, S.; Daniela, R. Polym Test 2001, 20, 409.
8. Maiti, S. N.; Mahapatro, P. K. Polym Compos 1998, 9, 291.
9. Tavman, I. H. Powder Technol 1997, 91, 63.
10. Thongruang, W.; Spontak, R. J.; Balik, C. M. Polymer 2002, 43, 2279.
11. Chan, C. M.; Wu, J.; Li, J. X.; Cheung, Y. K. Polymer 2002, 43, 2981.
12. Cheng, J.; Wang, G.; Zeng, X.; Zhao, H.; Cao, D.; Yun, J.; Tan, C. K. J Appl Polym Sci 2004, 94, 796.
13. Jeon, H. S.; Rameshwaram, J. K.; Kim, G.; Weinkauf, D. H. Polymer 2003, 44, 5749.
14. Hoffmann, B.; Dietrich, C.; Thomann, R.; Friedrich, C.; Mülhaupt, R. Macromol Rapid Commun 2000, 21, 57.
15. Karrad, S.; Cuesta, J. M. L.; Crespy, A. J Mater Sci 1998, 33, 453.
16. Wang, M.; Shen, Z.; Cai, C.; Ma, S.; Xing, Y. J Appl Polym Sci 2004, 92, 126.
17. Wu, G.; Song, Y.; Zheng, Q.; Du, M.; Zhang, P. J Appl Polym Sci 2002, 88, 2160.
18. Wong, W. K.; Ourieva, G.; Tse, M. F.; Wang, H. C. Macromol Symp 2003, 194, 175.
19. Demjén, Z.; Pukánszky, B.; Nagy, J. Compos A 1998, 29, 323.
20. Tabtiang, A.; Venables, R. Eur Polym J 2000, 36, 137.
21. Guillet, A. Macromol Symp 2003, 194, 63.

22. Doi, Y.; Kaneko, S.; Fujii, O. Jpn Kokai Tokkyo Koho Sho 52–156776 (1977).
23. Tanaka, S.; Yamuchi, K.; Kawai, S. Jpn Kokai Tokkyo Koho Sho 53–126319 (1978).
24. Kundu, P. P.; Choe, S. J Macromol Sci Rev 2003, 43, 143.
25. Nago, S.; Nakamura, S.; Mizutani, Y. J Appl Polym Sci 1992, 45, 1527.
26. Lee, J.; Macosko, C. W.; Blates, F. S. J Appl Polym Sci 2004, 91, 3642.
27. Kim, K. J.; Kwon, S.; Kim, H.; Kundu, P. P.; Kim, Y. W.; Lee, Y. K.; Lee, K. J.; Lee, B. H.; Choe, S. J Appl Polym Sci 2003, 87, 311.
28. Fried, J. R. Polymer Science and Technology; Prentice Hall PTR: Upper Saddle River, NJ, 1996.
29. Biswas, J.; Kim, H.; Yim, C. S.; Cho, J.; Kim, G. J.; Choe, S. Macromol Res 2004, 12, 443.
30. Lyu, S. G.; Ryu, J. G.; Sur, G. S.; Ahn, J. H. Korea Polym J 1997, 5, 173.
31. Suwanprateeb, J. Compos A 2000, 31, 353.
32. Premphet, K.; Horanont, P. J Appl Polym Sci 1999, 74, 3445.
33. Mizutani, Y.; Nakamura, S.; Kaneko, S.; Okamura, K. Ind Eng Chem Res 1993, 32, 221.
34. Narkis, M.; Nicolais, L. J Appl Polym Sci 1971, 15, 469.